Desalination and Water Treatment
www.deswater.com

doi: 10.5004/dwt.2019.23133

139 (2019) 145–155
January

Fabrication of quantum Cu(II) nanodot decorated TiO_2 nanotubes by the photochemical deposition-assisted hydrothermal method: study catalytic activity in hydrogen generation

Neda Gilani*, Javad Vahabzadeh Pasikhani, Parisa Tafazoli Motie, Mahmood Akbari

Fouman Faculty of Engineering, College of Engineering, University of Tehran, P.O. Box 43515-1155, Fouman 43516-66456, Iran, email: gilani@ut.ac.ir (N. Gilani), vahabzadeh089@gmail.com (J.V. Pasikhani), parisa_95t@yahoo.com (P.T. Motie), mahmood.akbari95@gmail.com (M. Akbari)

Received 23 April 2018; Accepted 13 September 2018

ABSTRACT

Nanotubular structures of TiO_2 were synthesized through a hydrothermal process and quantum Cu(II) nanodots (QCNs) were homogeneously deposited on their surface using a photo-deposition method. The surface morphology, structural properties, crystallography, elemental composition, surface chemistry and specific surface area of the synthesized samples were determined by the FESEM, TEM, XRD, EDS, FTIR and BET analysis, respectively. The results showed that dispersion of fine QCNs onto the TiO_2 nanotubes (TNTs) can dramatically increase their surface area from 86.54 to 644.29 m^2/g. Also, investigation of the catalytic performance of the prepared catalysts in generation of hydrogen from $NaBH_4$ revealed that QCN deposition enhances the catalytic activity of the TNTs. So that, application of 2wt.% QCN resulted in more than 2-fold increase (from 9 to 21.67 mL min^{-1}) in the rate of hydrogen production due to the provision of a high surface area and the synergistic effect between the QCNs and the TNTs. Kinetics studies on the $NaBH_4$ hydrolysis reaction catalyzed by QCNs (2%)/TNTs suggested that the reaction rate is first-order with respect to the catalyst amount and zero-order relative to $NaBH_4$ concentration Furthermore, the results of catalyst reusability showed that QCNs (2%)/TNTs is noticeably stable and quite active up to the fifth run.

Keywords: TiO_2 nanotubes; QUANTUM Cu(II) nanodots; Catalytic hydrolysis; $NaBH_4$

1. Introduction

High development of economy has led to an ever-increasing need of energy in the today's world. On the other hand, the concerns related to exhaustion of fossil fuel resources, environmental pollution and the global warming caused by the steep increase in the emission of carbon dioxide and other gases have motivated the application of hydrogen as a beneficial source of energy [1–4]. Hydrogen does not naturally exist in its energy rich state. However, it can be obtained from many different sources, such as water, ethanol, natural gas and other fossil fuels [5,6]. Among these sources, petroleum and natural gas are majorly used to generate hydrogen through steam reforming. However, this method requires consumption of energy and results in greenhouse gas emissions, mainly carbon dioxide [7]. In contrast, the chemical hydrogen storage can be adopted as a promising strategy of hydrogen production. In this approach, hydrogen is stored in chemical compounds, such as $NaBH_4$, NH_3BH_3, LiH, NaH, CaH_2, MgH_2 and $LiAlH_4$, and released via an irreversible chemical reaction [8,9]. Among these chemical hydrides, $NaBH_4$ is an attractive candidate owing to several advantages, including high hydrogen capacity (10.8 wt%), non-flammable, stabile solutions of alkaline, a simple controllable production rate of hydrogen, modest temperature of operation, and nontoxic hydrolysis byproducts [9,10]. To limit the $NaBH_4$ self-hydrolysis, NaOH is commonly inserted into the solution of $NaBH_4$ as stabilizer [11]. However, the hydrolysis of $NaBH_4$ systems at room temperature is quite slow and it can be completely suppressed by working in highly basic solution [12]. When compared with conventional production of hydrogen from aqueous $NaBH_4$, the catalytic hydrolysis of $NaBH_4$ in

*Corresponding author.

limited water amount can accelerate hydrogen generation rate [13]. Generally, the following stoichiometric equations are employed for hydrolysis of $NaBH_4$ [14]:

$$NaBH_4 + 4H_2O \rightarrow NaB(OH)_4 + 4H_2 \quad (1)$$

$$NaBH_4 + 2H_2O \xrightarrow{catalyst} NaBO_2 + 4H_2 \quad (2)$$

In this respect, noble metal-based catalysts containing Ru, Rh, Pt and Pd have been reported to promote $NaBH_4$ hydrolysis, considerably [13]. However, great costs, constrained reservoir or modest catalytic activity have limited the application of catalytic $NaBH_4$ hydrolysis processes in large scales [15]. Therefore, novel catalysts with lower costs and higher efficiencies should be developed. To date, metal oxides of Co, Cu, Ni, Zn, Fe, Ti, Al and many other metals have been widely studied due to their excellent physical and chemical properties [8]. Among them, Cu-based catalysts have attracted more attention since they exhibit a good level of activity and selectivity for hydrolysis of $NaBH_4$, their costs are lower than noble metals and they are environmentally friendly [16,17]. In addition, the study of Eugenio et al. [18] regarding the catalytic activity of Cu-Co foams has indicated that porous Cu-rich foams can be used as an alternative to Co-based catalysts to provide a low-cost, active and stable heterogeneous catalyst for production of hydrogen through sodium borohydride hydrolysis. The major drawback of copper based catalysts is that they dramatically lose their activity after only a few operative cycles due to the strong adsorption of byproducts, i.e. $B(OH)_4^-$, on their surface [19,20]. Moreover, such catalysts aggregate intensely across the reaction because of their high surface energy and cause a considerable catalytic activity deficiency [16]. Aggregation of Cu-based metal catalysts can be hindered by employing various support materials. The utilized support can immobilize bare metal nanoparticles (NPs) and reinforce their catalytic stability and activity [21–23].

Due to the effective role of catalyst supports, extensive efforts have been devoted to exploring new supporting materials. Specifically, TiO_2 has been widely studied for evolution of hydrogen since it has unique chemical and physical properties and exceptional stability. Furthermore, it is low-cost, nontoxic and abundant [24,25]. One of the key features in catalytic materials is their specific surface area, which needs to be sufficiently high. While TiO_2 can be found in many forms, TiO_2 nanotubes (TNTs) can provide open mesoporous morphology and the highest surface area for catalytic applications. In addition, the mesopores of TNTs facilitate diffusion of reagents towards active catalyst sites and, therefore, greatly improve the catalytic activity of different catalysts [25,26]. To the best of our knowledge, deposition of Cu NPs on TNTs (Cu/TNT) for generation of hydrogen from sodium borohydride has not been reported previously. Therefore, this study focuses on the synthesis and application of Cu/TNT.

To obtain a desired performance from the Cu/TNT catalyst, it is necessary to disperse fine Cu NPs onto the TNTs support. For this purpose, the photo-deposition technique is used as an appropriate method that can even be employed for deposition of quantum Cu (II) nanodots (QCNs) [27–31]. QCNs are a new and relatively homogeneous class of Cu nanomaterials with unique adsorption potential and excellent optical and electronic properties [32–34]. Deposition of QCNs on TNTs and catalytic performance of the resultant catalyst (QCNs/TNTs) for hydrolysis of $NaBH_4$ have not been reported, previously. Accordingly, the present study investigates the catalytic activity of QCNs/TNTs in hydrogen generation through $NaBH_4$ hydrolysis. For this purpose, TNTs are synthesized via a hydrothermal process and QCNs are deposited on them using a photo-deposition method. The produced catalysts are characterized by FESEM, TEM, XRD, FTIR and BET analysis. Furthermore, various variables including QCN concentration, catalyst dose, $NaBH_4$ amount and catalyst recyclability are evaluated to determine their effects on generation of hydrogen from $NaBH_4$.

2. Experimental

2.1. Catalyst preparation

In this research, the TNTs were synthesized through an ultrasound-assisted hydrothermal method. As the precursors of the TNTs, a commercial TiO_2 powder (P25, Evonik, Germany) and pellets of sodium hydroxide (Merck) were used without any further purification. First, 2 g of the commercial TiO_2 powder was added to 100 mL concentrated NaOH (10 M) and stirred for 30 min at room temperature to form a suspension. To homogenize the suspension, it was ultrasonicated for 30 min at room temperature. Then, the homogenized suspension was transferred to a Teflon vessel to carry out the hydrothermal reaction at 150°C for 48 h. After cooling down the reaction mixture to room temperature, the resultant white precipitates were separated and washed repeatedly with a dilute HCl solution (0.1 M) and distillated water until the pH of the solution reached a neutral state. After that, the hydrothermal products were separated from the washing solution by filtration and dried for 15 h at 80°C in an oven. Finally, the as-synthesized TNTs were calcined at 400°C in air for 2 h.

The QCNs/TNTs particles were prepared via an in situ photo-deposition method [27,35]. Accordingly, the as-prepared TNTs were first mixed with the required amount of aqueous $CuCl_2$ (0.01 M) under ultrasound irradiation. Then, N_2 was purged into the solution to remove the dissolved oxygen molecules. After that, 5 mL glycerol was injected into the suspension and the mixture was irradiated for 2 h with a 400 W UV lamp under magnetic stirring. The final product was filtered, washed, dried and calcined. Hereinafter, the obtained catalysts are called QCNs(x)/TNTs, where x is the nominal weight percentage of Cu in the final product (0.5%, 1%, 1.5% or 2%). Fig. 1 illustrates preparation of the QCNs(x)/TNTs catalysts, schematically.

2.2. Catalyst characterization

The prepared catalysts were analyzed using an X-ray diffraction (XRD) instrument (Philips X'Pert Pro X-ray

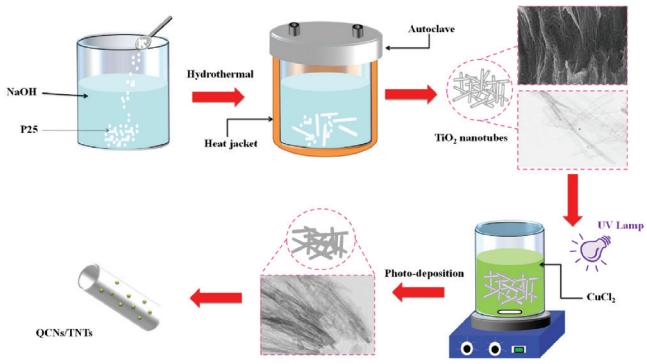

Fig. 1. Schematic representation of the catalyst synthesis method.

diffractometer, Germany) to obtain crystallographic information. The XRD patterns were collected by applying Cu Kα radiation (wavelength: 1.54 Å) over the 2θ range of 10–80. The surface morphology and structural features of the catalysts were studied using field-emission scanning electron microscopy (FESEM, TESCAN MIRA3-XMU, Czech Republic) and transmission electron microscopy (TEM, PhillipsFEGCM300, Germany), respectively. The elemental composition of the catalysts was identified by an energy-dispersive X-ray spectroscope (EDS, TESCAN MIRA3–XMU, Czech Republic) linked to the FESEM device. To determine the functional groups of the catalysts, Fourier transform infrared (FTIR) analysis (Bruker alpha-2000, USA) was performed over the wavenumber range of 500–4000 cm^{-1}. The Brunauer-Emmet-Teller (BET) analysis was carried out by a micrometer ASAP 2000 instrument (USA) to estimate the pore volume and the specific surface area of the catalysts. In addition, the mean value of pore size and pore distribution were estimated from the adsorption isotherms of the particles based on the Barrette-Joynere-Halenda (BJH) analysis method, which principally relies on multi-point isothermal adsorptions-desorption of nitrogen gas.

2.3. Hydrogen production

Activity of the as-prepared catalysts was investigated by applying them to the production of hydrogen through hydrolysis of sodium borohydride. In this investigation, 10 mL of a $NaBH_4$ solution containing 5 wt% $NaBH_4$ and 1.5 wt% NaOH was poured into a sealed flask and placed in a thermostatic water bath that was maintained at 30°C. To measure the volume of the hydrogen gas evolved from the reaction, a graduated burette (1000 mL) filled with water was attached to the reaction flask. Then, the catalyst particles (100 mg) were added to the sealed reaction flask and the flask contents were stirred at 800 rpm. Immediately, monitoring of the progress of the reaction started by measuring the produced hydrogen gas using the water displacement method. In this method, the volume of hydrogen was supposed to be equal to that of the displaced water, the weight of which was recorded by a balance. After the reaction, the catalyst particles were removed through filtration, completely rinsed and dried for 10 h at 60°C. Then the catalyst was reused for another cycle of hydrolysis. For reusability assessment of the optimal catalyst, the catalyzed hydrolysis reaction was repeated 5 times.

3. Results and discussion

3.1. XRD

The XRD patterns of the parent TNTs and the QCNs/TNTs catalysts containing various Cu quantities are depicted in Fig. 2. The TNT pattern presented in Fig. 2 unravels the presence of anatase TiO_2 (101) as the main phase at the 2θ value of 25.3°. Also, the diffraction peaks positioned at 37.9°, 48.1°, 53.8°, 55.2°, 62.2°, 68.8°, 70.02° and 75. 09° represent the other nanocrystalline phases of anatase TiO_2, which can be indexed as (004), (200), (105), (211), (213), (116), (220) and (215), respectively [36–39]. Comparison of the XRD patterns of the catalysts with that of TiO_2 declares that the inclusion of Cu has not led to any changes in the number and position of the TNT peaks. Moreover, Fig. 2 outlines no Cu oxide species. Therefore, it can be stated that the catalysts have conserved the anatase structure of TNT and the Cu species are highly dispersed on the surface of the TNTs.

The average crystallite size of the synthesized samples was estimated based on the line broadening of the XRD peak observed around 25.3°, i.e. the (101) plane, using the Scherer's equation:

$$D = \frac{k\lambda}{\beta\cos\theta} \tag{3}$$

where D is the average crystallite size, k is a constant (=0.89, here), λ is the wavelength of the X-ray radiation source (=1.5406 Å), θ is the Bragg's angle, and β is full width of the diffraction peak at half its maximum intensity in radian. Furthermore, the lattice parameters were obtained using the following equations [40]:

$$\text{Bragg's law: } 2d_{(hkl)} \sin\theta = \lambda \tag{4}$$

$$\frac{1}{d_{(hkl)}} = \frac{h^2}{a^2} + \frac{k^2}{b^2} + \frac{l^2}{c^2} \tag{5}$$

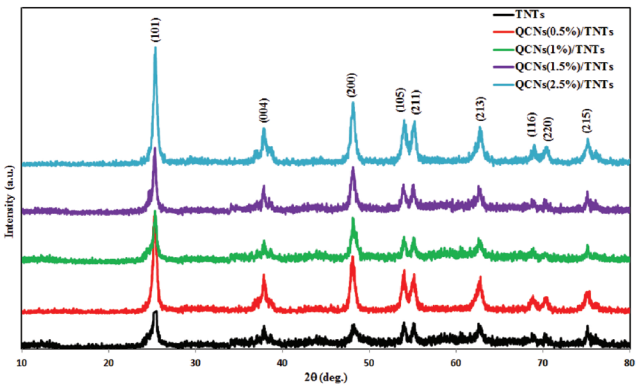

Fig. 2. The XRD patterns of the TiO_2 nanotubes and the catalysts calcined at 400°C in air.

where h, k and l are the crystal plane indices, $d_{(hkl)}$ is the distance between the (hkl) crystal planes, θ is the diffraction angle of the (hkl) crystal plane, and a, b, and c are lattice parameters (anatase crystal: $a = b \neq c$). Also, volume of the crystal cells (tetragonal) was calculated through Eq. (6).

$$v = a^2 c \tag{6}$$

The calculated crystal sizes, lattice parameters and cell volumes of the synthesized particles are reported in Table 1. With respect to Table 1, the values of the lattice parameters are in line with the anatase structure of TiO_2 (JCPDS card 21–1272). Also, the crystallite lattice of all samples, whose sizes range from 11.18 (TiO_2) to 20.13 nm (QCNs/TNTs), are nanosized. The crystallite size increase of TNT upon QCN incorporation can be justified since the ionic radius of Cu^{2+} (0.73 Å) is greater than that of Ti^{4+} (0.64 Å). In addition, Table 1 reveals a slight increase in the cell volume and lattice parameters of TNT by deposition of QCN. It is due to resemblance in Cu^{2+} and Ti^{4+} ionic radius allowing the interstitial incorporation and generating lactic strain in the network of TNT [41]. These results could infer the thorough dispersion of QCNs on the TiO_2 surfaces.

3.2. FESEM and TEM

Fig. 3 shows the FESEM and TEM images of the commercial TiO_2 powder, pure TNTs and QCNs (2%)/TNTs. The FESEM image of the commercial TiO_2 powder (Fig. 3a) displays non-uniform spherical particles whereas Fig. 3b depicts cylinder-like particles. Therefore, it can be concluded that the raw TiO_2 NPs have converted into nanotubular structures during the hydrothermal treatment. According to the TEM image of the TNTs (Fig. 3c), the average inner diameter and the wall thickness of the TNTs are 5.4 and 3.5 nm, respectively. By comparison of Fig. 3c with Fig. 3d, the 1–3 nm black dots that are appeared on the TNT particles can be assigned to the deposited QCNs.

Table 1
Phase, crystal size and lattice parameters of the prepared catalysts

Catalysts	Crystal phase	Crystallite size (nm)	$a = b$ (Å)	c (Å)	v (Å^3)
TNTs	Anatase	11.880	3.853	9.041	134.269
QCNs (0.5%)/TNTs	Anatase	20.125	3.785	9.463	135.605
QCNs (1%)/TNTs	Anatase	20.129	3.783	9.498	135.946
QCNs (1.5%)/TNTs	Anatase	20.129	3.786	9.451	135.492
QCNs (2%)/TNTs	Anatase	20.131	3.784	9.459	135.449

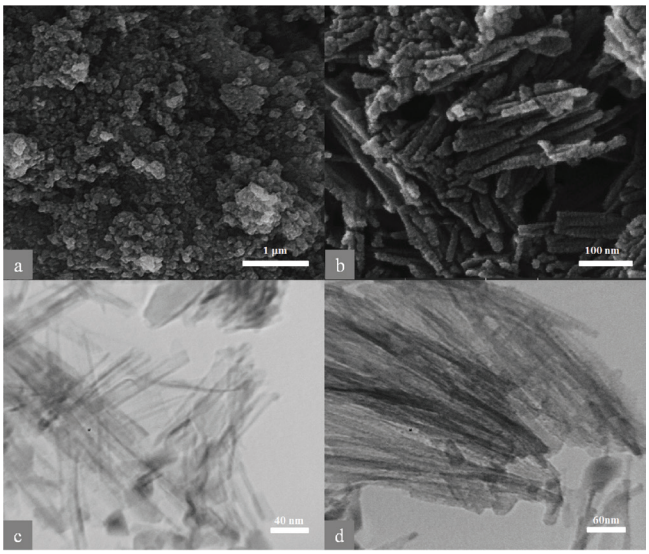

Fig. 3. The FESEM images of (a) the commercial TiO_2 powder and (b) the pure TiO_2 nanotubes, and the TEM images of (c) the pure TiO_2 nanotubes and (d) QCNs(2%)/TNTs.

3.3. Elemental EDS and mapping

Fig. 4 presents the EDS spectra of the as-prepared catalysts. The quantitative EDS results are given in Table 2. Based on Fig. 4(a) and Table 2, the TNTs contain 51.27% Ti, 41.52% O and 7.22% Na. The presence of copper in TiO_2 nanotubes was further confirmed by EDS analysis (Fig. 4). QCNs/TNTs catalyst mainly consisted of Ti, O, Na, and Cu. The EDS analysis of QCNs/TNTs shows a peak around 0.4 and 0.5 keV, and another intense peak appears at 4.5 and 4.9 keV for Ti. The peaks due to copper are clearly distinct at 0.9 and 8.0 keV. Since the characteristic peaks of Cu are evident in Fig. 4, the EDS spectra can be considered as a direct proof of successful QCN deposition onto the TNTs. Generally, the variations in the elemental composition of the samples (Table 2) suggest that QCNs are definitely present in the catalysts. Moreover, the experimental values of elemental percentages are close to the predicted values (Table 2).

X-ray elemental mapping was performed on the QCNs(2%)/TNTs catalyst to illuminate the distribution of QCNs on the surface of TNTs. Fig. 5 shows the obtained map. As this figure shows, the QCNs are homogeneously distributed on the surface of the TNTs.

Table 2
Elemental composition (%) of the prepared catalysts

Catalysts	O (w%)[a]	Na (w%)[a]	Ti (w%)[a]	Cu (w%)[a]	Cu (w%)[b]
TNTs	41.52	7.22	51.27	0	0
QCNs (0.5%)/TNTs	53.30	2.89	43.28	0.54	0.5
QCNs (1%)/TNTs	51.07	6.46	41.49	0.98	1
QCNs (1.5%)/TNTs	44.51	4.53	49.76	1.20	1.5
QCNs (2%)/TNTs	44.55	0.36	53.32	1.77	2

[a] Actual values determined by EDS analysis.
[b] Predicated values.

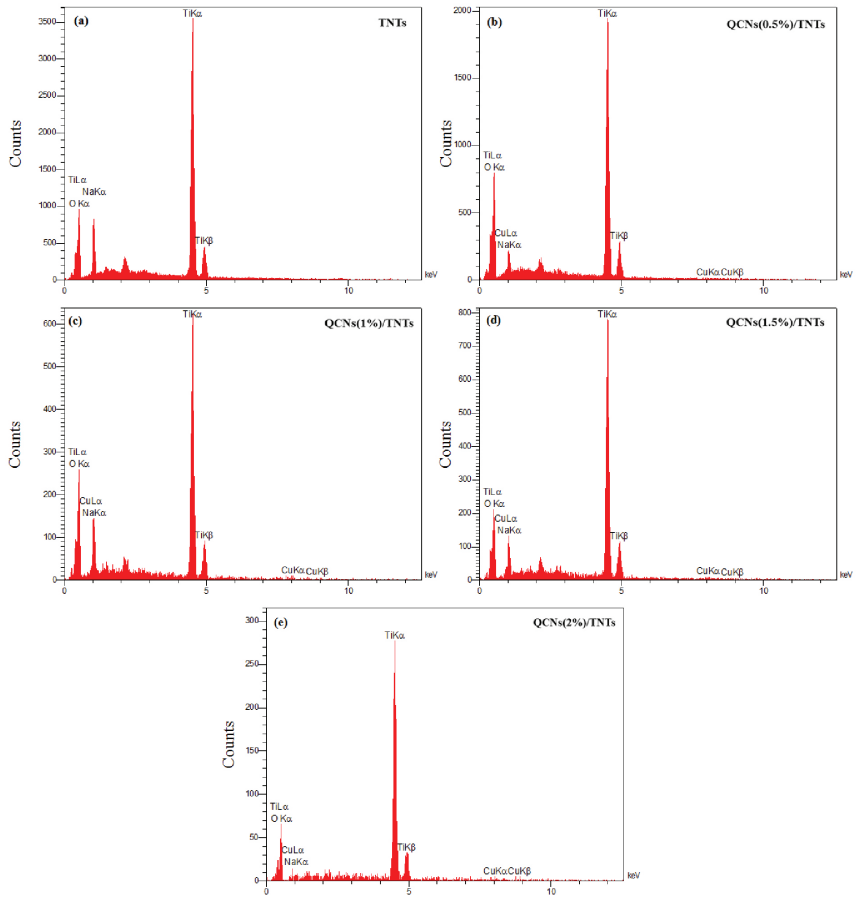

Fig. 4. The EDS spectra of (a) the pure TiO_2 nanotubes, (b) QCNs (0.5%)/TNTs, (c) QCNs (1%)/TNTs, (d) QCNs (1.5%)/TNTs, and (e) QCNs (2%)/TNTs.

3.4. FTIR

Fig. 6 exhibits the functional groups of the synthesized photocatalysts as indicated by FTIR spectroscopy. In this figure, the peaks observed around 3420 and 2962 cm^{-1} refer to the Ti–OH bonds [42]. Also, the spectra of all catalysts show a relatively strong band from 1635 to 1622 cm^{-1} that is due to the OH bending vibration of the water molecules chemisorbed and/or physisorbed on their surface [43]. The broad absorption peaks positioned from 800 to 700 cm^{-1} and from 490 to 433 cm^{-1} are related to the asymmetric stretching, symmetric stretching and the bending modes of the Ti–O–Ti bond, respectively [44]. For all photocatalysts, a small peak is observed around 3780 cm^{-1} that can be assigned to the O–H stretching of the hydroxyl group coordinated to the Ti atoms [42]. The broad low-intensity band that is risen around 840 cm^{-1} is indicative of Na–O–Ti bending of the sodium titanates [45]. The bands located at about 585 to 525 cm^{-1} are related to the low-frequency stretching vibrations of Cu–O and Cu–Ti. The bands that are just present in the FTIR spectra of the catalysts and are observed lower than 1100 cm^{-1} are related to the Cu–O bond vibrations [46]. Also, the vibrational bands observed at 1100 to 1360 cm^{-1} are associated with the Ti–O and Ti–OH stretching vibrations [44]. These results confirm that the Cu and Na species are incorporated into the TiO_2 nanotubes, in agreement with the EDS results.

3.5. BET

The structural characteristics and pore size distribution of the as-synthesized catalysts were evaluated via N_2 adsorption–desorption analysis. The corresponding isotherms and properties are presented in Fig. 7 and Table 3, respectively. As it can be seen, all samples have demonstrated typical type IV isotherms with an evident type-H3 hysteresis loop over the relative pressure (P/P0) range of 0.4 to 1.0, according to the IUPAC classification [47]. This kind of isotherm suggests a slit-like pore geometry formed by the TNTs due to their aggregation. Such geometry is typical for mesoporous materials [48]. Based on Fig. 7, the hysteresis loop of the catalysts becomes smaller with the increase of QCN amount and shifts towards the high relative pressure region of 0.8 to 1.0. The insets of Fig. 7 illustrate the pore size distributions of the catalysts. As exhibited in the insets of Fig. 7, the extent of copper deposition has a great impact on the pore size distribution of the catalysts. When the QCN content is less than or equal to 1 wt%, the pore size distributions of the catalyst particles is almost identical and relatively narrow with an average pore size around 12 nm. However, when loading of the QCN species increases to 2 wt%, the pore sizes distribute in a wider range (2–10 nm). Generally, deposition of QCNs on the pure TNTs increases their surface area and pore volume. In other words, the QCNs augment the surface attractive forces of the TNTs to

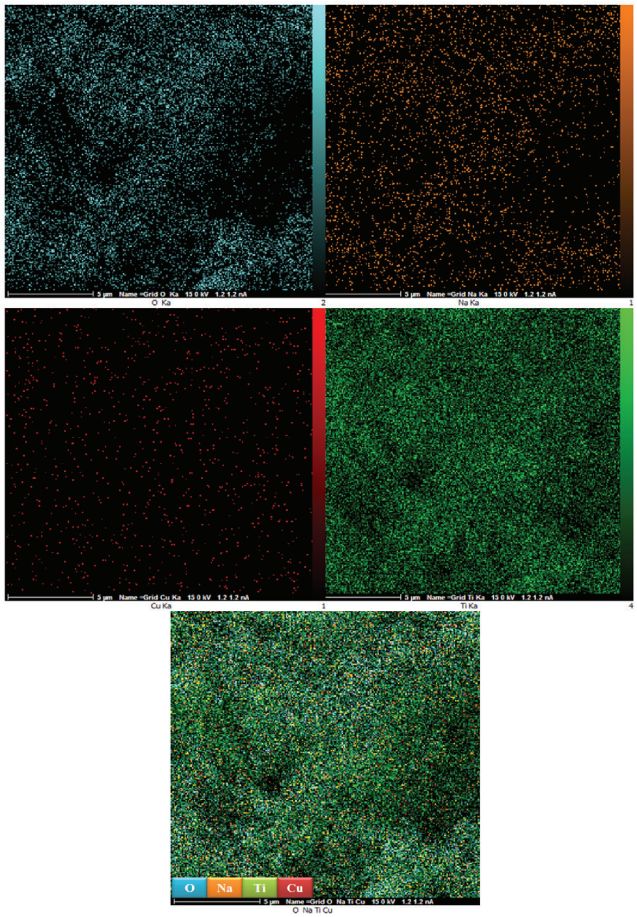

Fig. 5. The elemental mapping micrograph of the QCNs (2%)/TNTs catalyst.

form larger mesoporous pores without changing their pore type.

3.6. Catalytic performance of QCNs/TNTs

The performance of the synthesized catalysts was investigated by estimating the amount of hydrogen produced from hydrolysis of an alkaline $NaBH_4$ solution. The results of this experiment are shown in Fig. 8. After addition of the catalysts, hydrogen was released immediately without any induction period. The rate of hydrogen production (mL min^{-1}) was calculated with respect to the slopes obtained from the hydrogen volume–time curves. According to Fig. 8, TNT, itself, has some catalytic activity though it provides a low rate of hydrogen generation (9 mL min^{-1}) and gives just 113 mL H_2 within 15 min. This catalytic activity can be attributed to the acidic and basic sites of the TNTs. As Fig. 8 demonstrates, the catalytic activity of TNT can be enhanced by deposition of QCN on its surface. So that, increasing the amount of QCN improves the rate of hydrogen generation. For instance, adding 2 wt.% QCN to the TNTs can increase the rate from 9 to 21.67 mL min^{-1} and promote the amount of hydrogen produced within 15 min from 113 to 244 mL. This remarkable enhancement in the catalytic activity of TNT roots in to two factors. First, the newly added metal

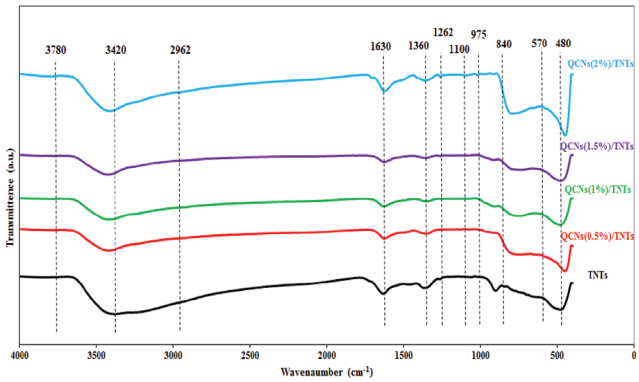

Fig. 6. The FTIR spectra of the TiO_2 nanotubes, QCNs (0.5%)/TNTs, QCNs (1%)/TNTs, QCNs (1.5%)/TNTs and QCNs (2%)/TNTs.

can act as an electrophile or Lewis acid for adsorption and activation of the reactants to increase the total rate of reaction. Second, deposition of QCN can increase the total surface area of TNT, dramatically (see Table 3). It should be noted that surface area is indirectly related to catalytic activity. The number of active sites in a catalyst with a high surface area is possibly greater than that of the same catalyst with less surface area. Consequently, deposition of more QCN species should result in promoted catalytic activity since it leads to enhanced surface area.

The origin of the superior catalytic activity of the QCNs/TNTs particles can be clarified by considering hydrolysis of borohydride over metal surfaces, as reported by Wu et al. [49]. Principally, the BH_4^- ions and H_2O molecules are activated on two different types of active sites. The reason is that BH_4^- activation requires an electron rich center while an electron deficient center is necessary for activation of H_2O. In the case of the QCNs/TNTs catalysts, there is a kind of acidic site on the surface of the TNTs, namely Lewis acid sites (exposed Ti^{n+} cations). These sites are stronger Lewis acids compared with the Cu ions [50]. Therefore, the water molecules should adsorb on the TNTs for activation while the BH4- ions should adsorb on the QCNs, as electron rich sites [51,52]. A possible pathway for QCNs/TNTs-based production of hydrogen from NaBH4 is illustrated in Fig. 9. In this reaction scheme, first H_2O and BH_4^- adsorb on the QCN and TNT sites, respectively. Then, a H^- ion transfers from BH_4^- to the Cu metal atom. The transferred hydrogen atom acquires an electron from the Cu metal to form the hydridic form of H^- while the created BH3–specie remains attached to the Cu atom [53]. At the same time, the adsorbed H_2O molecule coordinates to the unsaturated titanium atoms and/or interacts with the exposed surface oxygen atoms. This interaction leads to the polarization of the water molecule and, consequently, makes an H atom of H_2O more acidic [54]. Then, the reaction between the hydridic H^- ion of BH_4^- and the protic hydrogen of H_2O advances H_2 generation (II) and formation of surface adsorbed $BH_3(OH)^-$ as represented (III). In the next step, the cycle of charge transfer continues as $BH_3(OH)^- \rightarrow BH_2(OH)_2^- \rightarrow BH(OH)_3^- \rightarrow B(OH)_4^-$ and a H_2 molecule releases at each step. Thus, the superior catalytic performance of QCNs/TNTs can be ascribed to

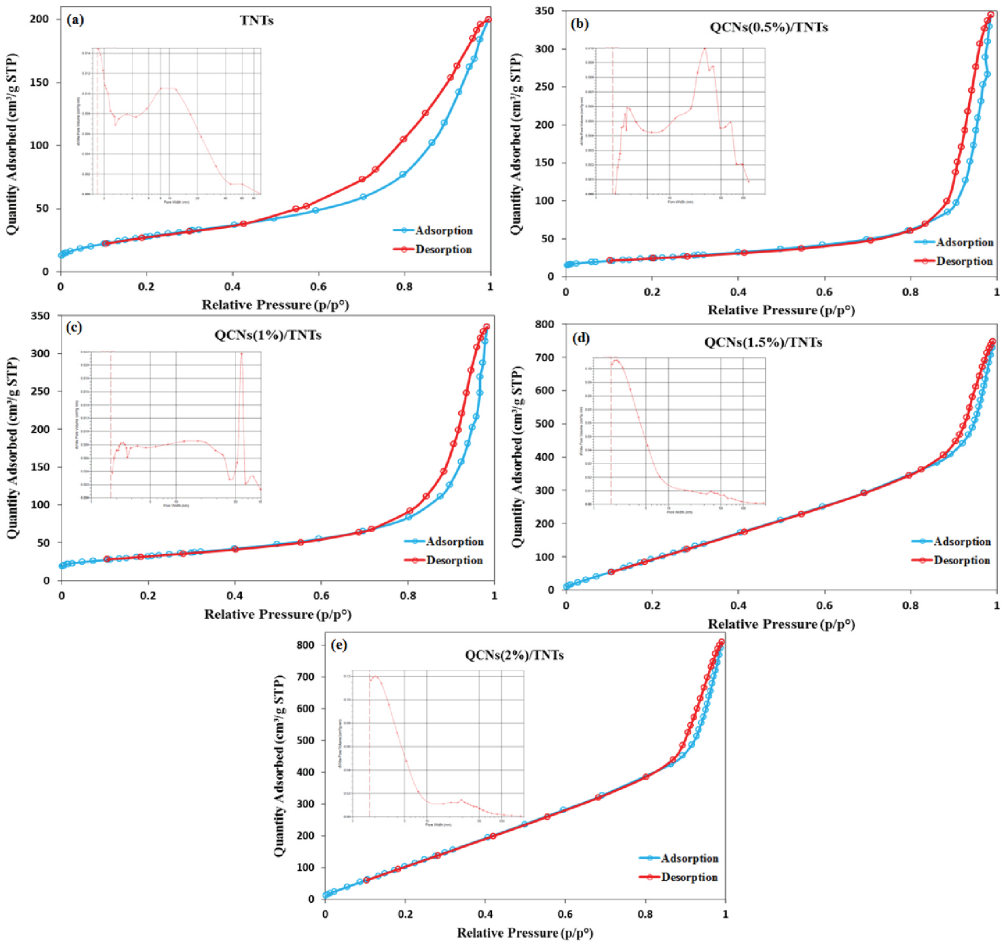

Fig. 7. The N_2 adsorption-desorption isotherms and pore size distributions of (a) the pure TiO_2 nanotubes, (b) QCNs (0.5%)/TNTs, (c) QCNs (1%)/TNTs, (d) QCNs (1.5%)/TNTs, and (e) QCNs (2%)/TNTs.

the high surface activity of the QCNs and the synergistic effect between the QCN species and the TNTs. Therefore, the results imply that the presence of QCNs on the surface of the TNTs increases the surface area of the TNTs and promotes its catalytic activity.

3.7. Effects of $NaBH_4$ concentration on hydrogen production

The effect of $NaBH_4$ concentration on the rate of hydrogen production was evaluated through a series of experiments starting with various initial concentrations of $NaBH_4$ (from 1 to 10 wt.%) while keeping the concentration of NaOH constant at 1.5 wt.% and using the same amount and type of catalyst (100 mg QCNs(2%)/TNTs). Figs. 10a and 10b illustrate the effect of sodium borohydride concentration on the rate and volume of hydrogen generation, respectively. Based on Fig. 10a, the volume of H_2 increases remarkably with the increase of $NaBH_4$ concentration from 1 to 5 wt.% and, then, decreases with further increase of the NaBH4 concentration to 10 wt%. It means that the application of excessive $NaBH_4$ concentrations is unfavorable for H_2 generation. The reason is that, at lower $NaBH_4$ concentrations, more BH_4^- ions and H_2O molecules would contact the active catalyst sites to generate more hydrogen molecules by provision of more $NaBH_4$ molecules. However, the generation of hydrogen is also accompanied with the formation of $NaBO_2$, which accumulates on the surface of the catalyst particles due to its low solubility under alkaline condition. Therefore, if the concentration of $NaBH_4$ be increased beyond a limit, the active sites of the catalyst would be blocked by the $NaBO_2$ products, solution viscosity would increase and mass transfer would be restricted [10,15]. Interestingly, Fig. 10b shows no obvious change in the rate of hydrogen generation with the increase of $NaBH_4$ concentration. This indicates that the hydrolysis of $NaBH_4$ by the QCNs (2%)/TNTs catalyst does not depend on the concentration of $NaBH_4$, which suggests that the hydrolysis reaction is zero-order reaction with respect to $NaBH_4$ concentration. A similar observation has been also reported about catalysis of the hydrolysis reaction by Co–B–TiO_2 framework [9] and Ag-activated TiO_2 [55].

3.8. Effects of catalyst dose on hydrogen production

To optimize the dose of the catalyst, hydrolysis of the alkaline $NaBH_4$ solution was monitored at 30°C using different amounts of the QCNs (2%)/TNTs catalyst (50–200

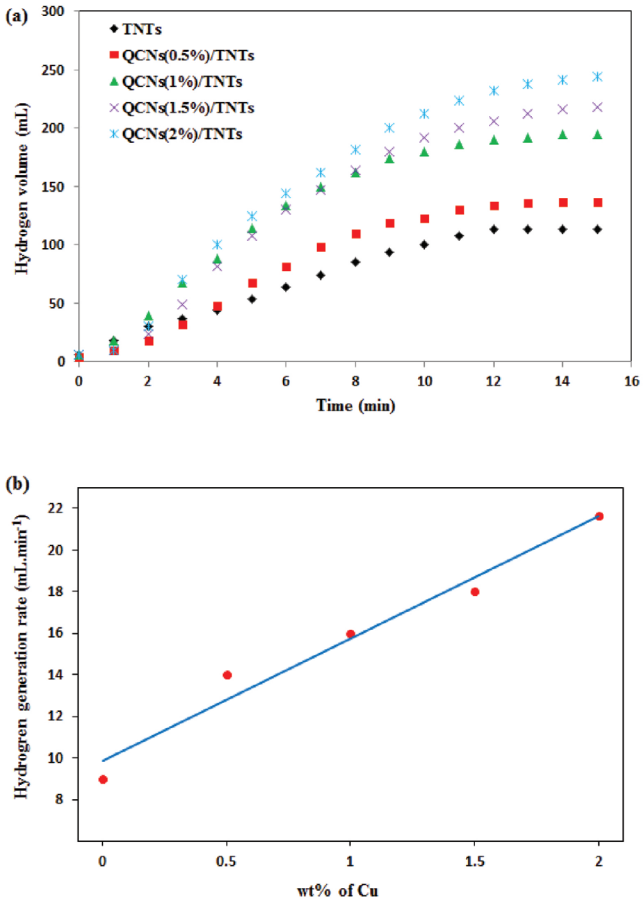

Fig. 8. Effect of the QCN content of the QCNs/TNTs catalysts on the volume (a) and rate (b) of hydrogen generation.

Table 3
Surface area and total pore volume of the prepared catalysts

Catalysts	Surface area (m^2/g)	Pore volume (cm^3/g)
TNTs	86.54	0.25
QCNs (0.5%)/TNTs	104.46	0.29
QCNs (1%)/TNTs	115.63	0.31
QCNs (1.5%)/TNTs	587.45	0.79
QCNs (2%)/TNTs	644.29	0.92

mg). The obtained results are displayed in Fig. 11. As shown in Fig. 11, increasing the dose of the catalyst improves hydrogen production. So that, generation of hydrogen within 15 min reaction promotes from 140 to 426 mL by the increase of catalyst dose from 50 to 200 mg (Fig. 11a). Fig. 11b plots the rate of hydrogen generation versus catalyst. This plot has given a fitted straight line (slope of 1.01) with a 0.9675 correlation coefficient (R^2). This result clearly shows that the rate of the catalyzed reaction is first-order with respect to the catalyst amount. Similar results have been reported about the CoB–TiO_2 [9], Cu–Fe–B [56] and Ag-activated TiO_2 [55] catalysts.

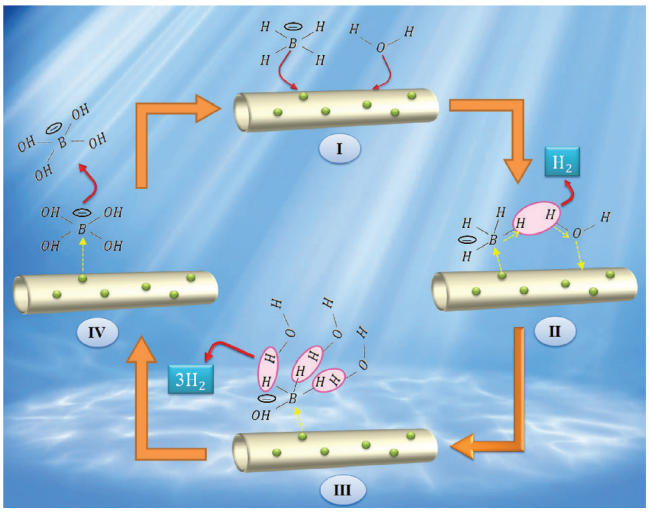

Fig. 9. The mechanism proposed for catalytic hydrolysis of $NaBH_4$ by the QCNs/TNTs catalysts.

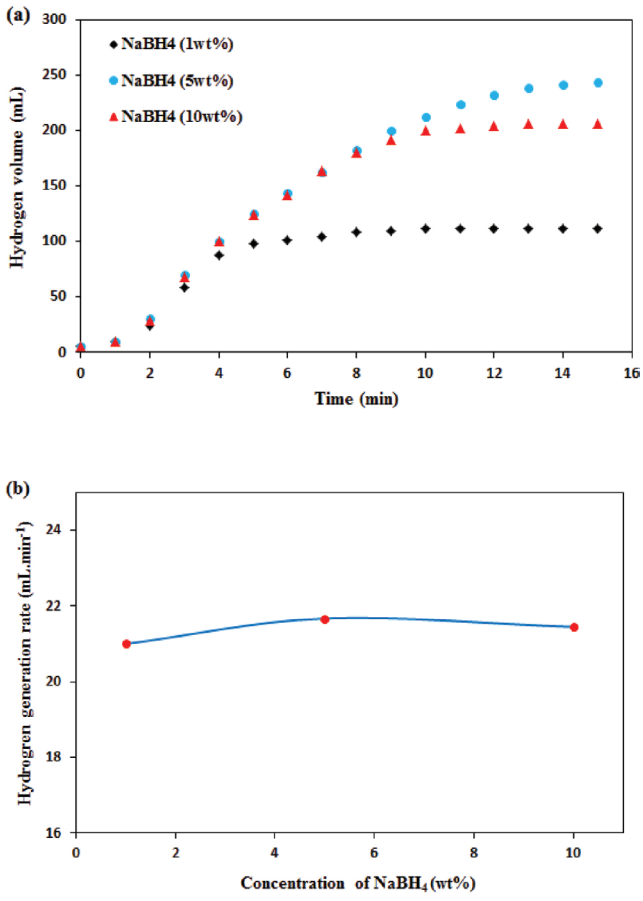

Fig. 10. Effect of $NaBH_4$ concentration on the volume (a) and rate (b) of hydrogen generation.

3.9. Catalyst recoverability

Catalyst reusability and stability are two important factors that should be considered for practical application

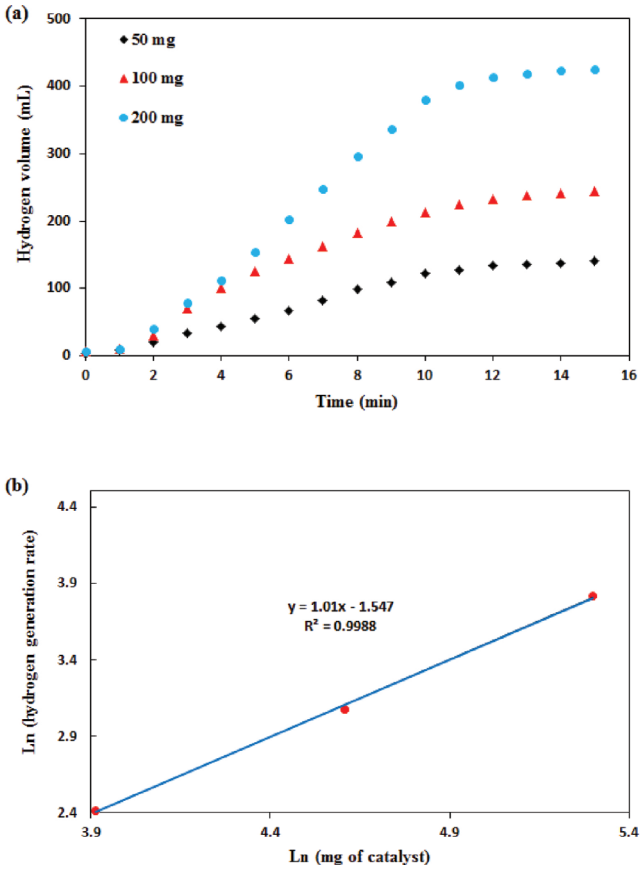

Fig. 11. Effect of QCNs (2%)/TNTs dose on the volume (a) and rate (b) of hydrogen generation.

of a hydrogen production system. Herein, to investigate stability of the QCNs (2%)/TNTs catalyst, the hydrolysis experiment was repeated 5 times using the same catalyst particles. After each cycle, the utilized catalyst was separated from the solution, rinsed completely with deionized water, dried and reused in the next cycle of $NaBH_4$ hydrolysis under the same reaction conditions. The results are exhibited in Fig. 12 and declare that the activity of QCNs (2%)/TNTs does not decline significantly after five consecutive runs. Therefore, this catalyst can be accepted as a recyclable catalyst for hydrolysis of $NaBH_4$.

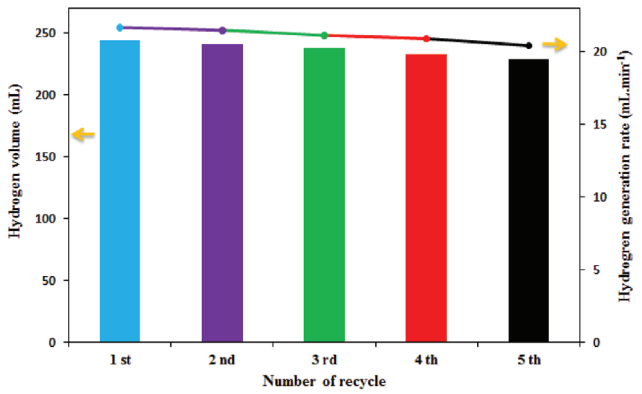

Fig. 12. Reusability of the QCNs (2%)/TNTs catalyst in $NaBH_4$ hydrolysis.

4. Conclusion

TiO_2 nanotubes were synthesized using a hydrothermal method and different amounts of quantum Cu nanodots (QCNs) were successfully deposited on them via a photo-deposition method. The performance of the resultant QCNs/TNTs catalysts was investigated in generation of hydrogen through $NaBH_4$ hydrolysis. The results showed that the presence of the deposited QCNs with 1 to 3 nm size has a dramatic influence on the surface area and hydrogen production rate of the TiO_2 nanotubes. So that, increasing the QCN content of the QCNs/TNTs catalyst led to an increase in the surface area of the TiO_2 nanotubes and an enhancement in the rate of hydrogen production. Among the examined QCNs/TNTs catalysts, the catalyst containing 2 wt% of QCN exhibited the best catalytic performance and produced 244 mL hydrogen at 30°C with the rate of 21.67 mL min^{-1}. Moreover, the kinetics studies indicated that the reaction rate of $NaBH_4$ hydrolysis catalyzed by QCNs (2%)/TNTs is first-order and zero-order with respect to the catalyst and $NaBH_4$, respectively. Furthermore, the QCNs (2%)/TNTs catalyst was reused for five times without any significant loss of catalytic activity and demonstrated high stability. According to the findings of this study, supporting QCNs on TiO_2 nanotubes can facilitate fabrication of catalysts for enhanced generation of hydrogen from $NaBH_4$ hydrolysis.

Acknowledgments

The authors would like to acknowledge the College of Engineering, University of Tehran for esteemed financial support.

References

[1] M.M. Momeni, Y. Ghayeb, Z. Ghonchegi, Visible light activity of sulfur-doped TiO_2 nanostructure photoelectrodes prepared by single-step electrochemical anodizing process, J. Solid State Electrochem., 19 (2015) 1359–1366.
[2] M.M. Momeni, M. Hakimian, A. Kazempour, Preparation and characterization of manganese–TiO_2 nanocomposites for solar water splitting, Surf. Eng., 32 (2016) 514–519.
[3] M.M. Momeni, Y. Ghayeb, Fabrication, characterization and photoelectrochemical performance of chromium-sensitized titania nanotubes as efficient photoanodes for solar water splitting, J. Solid State Electrochem., 20 (2015) 683–689.
[4] M.M. Momeni, Y. Ghayeb, M. Shafiei, Preparation and characterization of CrFeWTiO_2 photoanodes and their photoelectrochemical activities for water splitting, Dalton Trans., 46 (2017) 12527–12536.
[5] M.M. Momeni, Y. Ghayeb, Photoinduced deposition of gold nanoparticles on TiO_2-WO_3 nanotube films as efficient photoanodes for solar water splitting, Appl. Phys. A, 122 (2016).
[6] M.M. Momeni, Y. Ghayeb, F. Ezati, Fabrication, characterization and photoelectrochemical activity of tungsten-copper co-sensitized TiO_2 nanotube composite photoanodes, J. Colloid Interface Sci., 514 (2018) 70–82.
[7] M. Hakamizadeh, S. Afshar, A. Tadjarodi, R. Khajavian, M.R. Fadaie, B. Bozorgi, Improving hydrogen production via water splitting over Pt/TiO_2/activated carbon nanocomposite, Int. J. Hydrogen Energy, 39 (2014) 7262–7269.

[8] A.H. Tamboli, A.A. Chaugule, F.A. Sheikh, W.J. Chung, H. Kim, Synthesis and application of CeO_2-NiO loaded TiO_2 nanofiber as novel catalyst for hydrogen production from sodium borohydride hydrolysis, Energy, 89 (2015) 568–575.
[9] J. Cheng, C. Xiang, Y. Zoun, H. Chu, S. Qiu, H. Zhang, L. Sunnn, F. Xu, Highly active nanoporous Co–B–TiO_2 framework for hydrolysis of $NaBH_4$, Ceram. Int., 41 (2015) 899–905.
[10] O. Sahin, M.S. Izgi, E. Onat, C. Saka, Influence of the using of methanol instead of water in the preparation of Co-Be-TiO_2 catalyst for hydrogen production by $NaBH_4$ hydrolysis and plasma treatment effect on the Co-BeTiO_2 catalyst, Int. J. Hydrogen Energy, 41 (2016) 2539–2546.
[11] Y.R. Liu, X. Li, G.Q. Han, B. Dong, W.H. Hu, X. Shang, Y.M. Chai, Y.Q. Liu, C.G. Liu, Template-assisted synthesis of highly dispersed MoS_2 nanosheets with enhanced activity for hydrogen evolution reaction, Int. J. Hydrogen Energy, 42 (2017) 2054–2060.
[12] W. Ploysuksai, P. Rangsunvigit, S. Kulprathipanja, Effects of TiO_2 and Nb_2O_5 on Hydrogen Desorption of Mg $(BH_4)_2$, Int. J. Chem. Biol. Eng., 6 (2012) 328–332.
[13] S.S. Muir, X. Yao, Progress in sodium borohydride as a hydrogen storage material: Development of hydrolysis catalysts and reaction systems, Int. J. Hydrogen Energy, 36 (2011) 5983–5997.
[14] N. Sahiner, A.O. Yasar, N. Aktas, Metal-free pyridinium-based polymeric ionic liquids as catalyst for H_2 generation from $NaBH_4$, Renewable Energy, 101 (2017) 1005–1012.
[15] Z. Li, H. Li, L. Wang, T. Liu, T. Zhang, G. Wang, G. Xie, Hydrogen generation from catalytic hydrolysis of sodium borohydride solution using supported amorphous alloy catalysts (Ni-Co-P/g-Al_2O_3), Int. J. Hydrogen Energy, 39 (2014) 14935–14941.
[16] O. Sahin, D. Kılınc, C. Saka, Bimetallic Co-Ni based complex catalyst for hydrogen production by catalytic hydrolysis of sodium borohydride with an alternative approach, J. Energy Inst., 89 (2016) 617–626.
[17] C. Saka, O. Sahin, H. Demir, A. Karabulut, A. Sarikaya, Hydrogen Generation from Sodium Borohydride Hydrolysis with a Cu–Co-Based Catalyst: A Kinetic Study, Energy Sources, Part A: Recovery, Utilization, and Environmental Effects, 37 (2015) 956–964.
[18] S. Eugenio, U.B. Demirci, T. M. Silva, M.J. Carmezim, M.F. Montemor, Copper-cobalt foams as active and stable catalysts for hydrogen release by hydrolysis of sodium borohydride, Int. J. Hydrogen Energy, 41 (2016) 8438–8448.
[19] A. Koska, N. Toshikj, S. Hoett, L. Bernaud, U.B. Demirci, Volcano plot for bimetallic catalysts in hydrogen generation by hydrolysis of sodium borohydride, J. Chem. Educ., 94 (2017) 1163–1166.
[20] A. Marchionni, M. Bevilacqua, J. Filippi, M.G. Folliero, M. Innocenti, A. Lavacchi, H.A. Miller, M.V. Pagliaro, F. Vizza, High volume hydrogen production from the hydrolysis of sodium borohydride using a cobalt catalyst supported on a honeycomb matrix, J. Power Sources, 299 (2015) 391–397.
[21] H.A. Bandal, A.R. Jadhav, H. Kim, Cobalt impregnated magnetite-multiwalled carbon nanotube nanocomposite as magnetically separable efficient catalyst for hydrogen generation by $NaBH_4$ hydrolysis, J. Alloys Compd., 699 (2017) 1057–1067.
[22] Y. Chen, Y. Shi, X. Liu, Y. Zhang, Preparation of polyvinylidene fluoride–nickel hollow fiber catalytic membranes for hydrogen generation from sodium borohydride, Fuel, 140 (2015) 685–692.
[23] Y. Guo, J. Qian, A. Iqbal, L. Zhang, W. Liu, W. Qin, Pd nanoparticles immobilized on magnetic carbon dots@Fe_3O_4 nanocubes as a synergistic catalyst for hydrogen generation, Int. J. Hydrogen Energy, 42 (2017) 15167–15177.
[24] M.M. Momeni, I. Ahadzadeh, A. Rahmati, Nitrogen, carbon and iron multiple-co doped titanium dioxide nanotubes as a new high-performance photo catalyst, J. Mater. Sci.: Mater. Electron., 27 (2016) 8646–8653.
[25] Y. Ma, X. Li, Y. Zhang, L. Chen, J. Wu, D. Gao, J. Bi, G. Fan, Ruthenium nanoparticles supported on TiO_2 (B) nanotubes: Effective catalysts in hydrogen evolution from the hydrolysis of ammonia borane, J. Alloys Compd., 708 (2017) 270–277.
[26] S. Chen, C. Ostrom, A. Chen, Functionalization of TiO_2 nanotubes with palladium nanoparticles for hydrogen sorption and storage, Int. J. Hydrogen Energy, 38 (2013) 14002–14009.
[27] M. Zhang, R. Sun, Y. Li, Q. Shi, L. Xie, J. Chen, X. Xu, H. Shi, W. Zhao, High H_2 Evolution from Quantum Cu(II) Nanodot-Doped Two- Dimensional Ultrathin TiO_2 Nanosheets with Dominant Exposed {001} Facets for Reforming Glycerol with Multiple Electron Transport Pathways, J. Phys. Chem. C, 120 (2016) 10746–10756.
[28] M.M. Momeni, Fabrication of copper decorated tungsten oxide–titanium oxide nanotubes by photochemical deposition technique and their photocatalytic application under visible light, Appl. Surf. Sci., 357 (2015) 160–166.
[29] M.M. Momeni, N. Mohammadi, M. Mirhosseini, Photo catalytic property of Pt-CuO nanostructure films prepared by wet-chemical route and photochemical deposition method, J. Mater. Sci.: Mater. Electron., 27 (2016) 10147–10156.
[30] M.M. Momeni, Y. Ghayeb, Preparation of cobalt coated TiO_2 and WO_3–TiO_2 nanotube films via photo-assisted deposition with enhanced photocatalytic activity under visible light illumination, Ceram. Int., 42 (2016) 7014–7022.
[31] M.M. Momeni, I. Ahadzadeh, Copper photodeposition on titania nanotube arrays and study of their optical and photocatalytic properties, Mater. Res. Innovations, 20 (2016) 44–50.
[32] M. Kominkova, V. Milosavljevic, P. Vitek, H. Polanska, K. Cihalova, S. Dostalova, V. Hynstova, R. Guran, P. Kopel, L. Richtera, M. Masarik, M. Brtnicky, J. Kynicky, O. Zitka, V. Adam, Comparative study on toxicity of extracellularly biosynthesized and laboratory synthesized CdTe quantum dots, J. Biotechnol., 241 (2017) 193–200.
[33] H. Hosseinzadeh, N. Bahador, Novel CdS quantum dots templated hydrogel nanocomposites: Synthesis, characterization, swelling and dye adsorption properties, J. Mol. Liq., 240 (2017) 630–641.
[34] T. Yang, Y.K. Li, M.L. Chen, J.H. Wang, Supported carbon dots decorated with metallothionein for selective cadmium adsorption and removal, Chin. Chem. Lett., 26 (2015) 1496–1501.
[35] M. Hamadanian, S. Karimzadeh, V. Jabbari, D. Villagrán, Synthesis of cysteine, cobalt and copper-doped TiO_2 nanophotocatalysts with excellent visible-light-induced photocatalytic activity, Mater. Sci. Semicond. Process., 41 (2016) 168–176.
[36] J.V. Pasikhani, N. Gilani, A.E. Pirbazari, The effect of the anodization voltage on the geometrical characteristics and photocatalytic activity of TiO_2 nanotube arrays, Nano-Struct. Nano-Objects, 8 (2016), 7–14.
[37] M.M. Momeni, Y. Ghayeb, Synthesis and characterization of iron-doped titania nanohoneycomb and nanoporous semiconductors by electrochemical anodizing method as good visible light active photocatalysts, J. Mater. Sci.: Mater. Electron., 26 (2015) 5509–5517.
[38] M.M. Momeni, Y. Ghayeb, Photochemical deposition of platinum on titanium dioxide–tungsten trioxide nanocomposites: an efficient photocatalyst under visible light irradiation, J. Mater. Sci.: Mater. Electron., 27 (2015) 1062–1069.
[39] M.M. Momeni, Y. Ghayeb, M. Davarzadeh, Electrochemical construction of different titania–tungsten trioxide nanotubular composite and their photocatalytic activity for pollutant degradation: a recyclable photocatalysts, J. Mater. Sci.: Mater. Electron., 26 (2014) 1560–1567.
[40] N.N. Ilkhechi, M. Alijani, B.K. Kaleji, Optical and structural properties of TiO_2 nanopowders with Co/Ce doping at various temperature, Opt. Quantum Electron., 148 (2016), 1–9.
[41] R. Bashiri, N.M. Mohamed, C. F. Kait, S. Sufian, Hydrogen production from water photosplitting using Cu/TiO_2 nanoparticles: Effect of hydrolysis rate and reaction medium, Int. J. Hydrogen Energy, 40 (2015) 6021–6037.
[42] A.E. Pirbazari, P. Monazzam, B.F. Kisomi, Co/TiO_2 nanoparticles: preparation, characterization and its application for photocatalytic degradation of methylene blue, Desalin. Water Treat., 63 (2017) 283–292.

[43] P. Dashora, C. Ameta, R. Ameta, S.C. Ameta, Dye-sensitized solar cell using copper and nitrogen co-doped titania as photoanode, Int. J. Sustainable Green Energy, 4 (2015) 219–226.
[44] J.V. Pasikhani, N. Gilani, A.E. Pirbazari, The correlation between structural properties, geometrical features, and photoactivity of freestanding TiO_2 nanotubes in comparative degradation of 2,4–dichlorophenol and methylene blue, Mater. Res. Express, 5 (2018) 025016.
[45] D. Tsiourvas, A. Tsetsekou, M. Arkas, S. Diplas, E. Mastrogianni, Covalent attachment of a bioactive hyperbranched polymeric layer to titanium surface for the biomimetic growth of calcium phosphates, J. Mater. Sci.: Mater. Med., 22 (2011) 85–96.
[46] S.M. Reda, M. Khairy, M.A. Mousa, Photocatalytic activity of nitrogen and copper doped TiO_2 nanoparticles prepared by microwave-assisted sol-gel process, Arabian J. Chem., (2017), 1–10.
[47] M. Thommes, K. Kaneko, A.V. Neimark, J.P. Olivier, F. Rodriguez-Reinoso, J. Rouquerol, K.S.W. Sing, Physisorption of gases, with special reference to the evaluation of surface area and pore size distribution (IUPAC Technical Report), Pure Appl. Chem., 87 (2015) 1051–1069.
[48] M.M. Labani, R. Rezaee, A. Saeedi, A.A. Hinai, Evaluation of pore size spectrum of gas shale reservoirs using low pressure nitrogen adsorption, gas expansion and mercury porosimetry: A case study from the Perth and Canning Basins, Western Australia, J. Pet. Sci. Eng., 112 (2013) 7–16.
[49] Z. Wu, X. Mao, Q. Zi, R. Zhang, T. Dou, A.C.K. Yip, Mechanism and kinetics of sodium borohydride hydrolysis over crystalline nickel and nickel boride and amorphous nickel-boron nanoparticles, J. Power Sources, 268 (2014) 596–603.
[50] K. Bhattacharyya, A. Danon, B.K. Vijayan, K.A. Gray, P.C. Stair, E. Weitz, Role of the surface lewis acid and base sites in the adsorption of CO_2 on titania nanotubes and platinized titania nanotubes: an in situ FT-IR study, J. Phys. Chem. C, 117 (2013) 12661–12678.
[51] Y. Harima, T. Fujita, Y. Kano, I. Imae, K. Komaguchi, Y. Ooyama, J. Ohshita, Lewis-acid sites of TiO_2 surface for adsorption of organic dye having pyridyl group as anchoring unit, J. Phys. Chem. C, 117 (2013) 16364–16370.
[52] L.H. Mendoza-Huizar, D.E.G. Rodríguez, C.H. Rios-Reyes, A. Alatorre-Ordaz, Theoretical quantum study about the adsorption of BH_4^- onto X(100) where (X = Cu, Ag and Au), J. Mex. Chem. Soc., 56 (2012) 302–310.
[53] G. Guella, C. Zanchetta, B. Patton, A. Miotello, New insights on the mechanism of palladium-catalyzed hydrolysis of sodium borohydride from ^{11}B NMR measurements, J. Phys. Chem. B, 110 (2006) 17024–17033.
[54] Z. Futera, N.J. English, Electric-field effects on adsorbed-water structural and dynamical properties at rutile- and anatase-TiO_2 surfaces, J. Phys. Chem. C, 120 (2016) 19603–19612.
[55] X. Shen, Q. Wang, Q. Wu, S. Guo, Z. Zhang, Z. Sun, B. Liu, Z. Wang, B. Zhao, W. Ding, CoB supported on Ag-activated TiO_2 as a highly active catalyst for hydrolysis of alkaline $NaBH_4$ solution, Energy, 90 (2015) 464–474.
[56] A.F. Shojaei, M. Khakzad, M.H. Loghmani, Hydrogen generation as a clean energy through hydrolysis of sodium borohydride over Cu-Fe-B nano powders; effect of polymers and surfactants, Energy, 126 (2017) 830–840.